CONFERENCE PRE-PRINT

NONLOCAL BEHAVIOR OF TURBULENCE IN THE PRESENCE OF POLOIDALLY LOCALIZED HEAT SOURCE

September 29, 2025

Y.W. Cho*, X. Garbet, K. Lim, Z.S. Qu, R. Varennes School of Physical and Mathematical Science, Nanyang Technological University Singapore, Singapore Email: youngwoo.cho@ntu.edu.sg

Y. Sarazin, G. DIf-Pradalier, P. Donnel, K. Obrejan, V. Grandgirard CEA, IRFM F-13108 Saint-Paul-Lez-Durance, France

Abstract

Turbulence spreading from edge to core has been studied by means of global full-F gyrokinetic simulations with the GYSELA code. Our study focuses on understanding how the poloidal location of edge heating influences nonlocal transport characteristics and turbulence spreading. Low field side heating effectively excites turbulent fluctuations that propagate towrads the core and edge, with $E \times B$ shear layer radially shifting during the turbulence spreading. In contrast, high field side heating produces highly localized fluctuations with minimal spreading due to in-out asymmetry of $E \times B$ shearing rate and broader pressure perturbations at low field side.

1. INTRODUCTION

To improve confinement in tokamak plasmas, it is important to understand the nonlocal transport, such as turbulence spreading. Turbulence spreading is the process in which turbulence intensity is spatially redistributed through nonlinear coupling of turbulent fluctuations[1–6]. It is intrinsically non-diffusive and exhibits self-similar front propagation of fluctuations[2]. Turbulence spreading can be responsible for transport scale deviations from gyroBohm, which can even lead to Bohm scaling[3]. Turbulence spreading and the following transition of transport scale has been addressed by several global gyrokinetic simulations from GTC[7, 8], ORB5, GENE[9], gKPSP[10, 11], and GYSELA[12].

The region that particularly draws attention for nonlocal behavior is the so-called "No man's land," which corresponds to the connection region between the edge and core[13]. In this region, transport stronger than that measured by conventional local estimations has been observed. Recently, research on turbulence spreading from

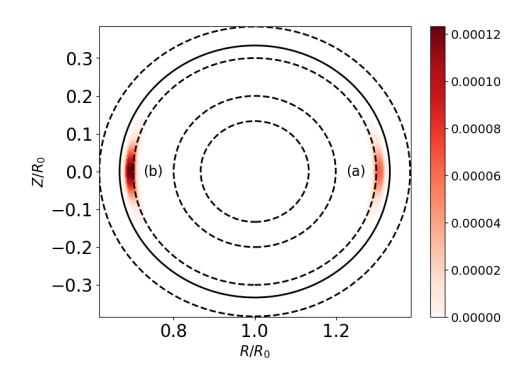


FIG. 1. Locations of poloidally localized heat sources. Dashed lines represent r/a = 0.4, 0.6, 0.9, 1.15, respectively. Bold line represents r/a = 1.0.

the edge to the core has been actively conducted to understand the transport level in this region[12, 14]. Indeed, devices such as DIII-D have measured the propagation of turbulent pulses from the edge to the core[15].

Recent research using GYSELA, a global full-F gyrokinetic code, has shown that time-modulated heat source can be utilized to analyze non-local transport event[16]. It shows that a localized and time-modulated heat source can trigger both diffusive and avalanche-like transport events. Note that nonlocal transport events triggered by this source exhibits correlation, such that propagation speeds of both heat and turbulent pulse are proportional to the frequency of heat source. This research suggests the possible application of localized heat source to study on nonlocal transport.

Inspired by these results, we employ GYSELA to investigate the nonlocal behavior of ITG turbulence and heat pulse propagation in response to poloidally localized heat source at the edge. We focus on understanding how the poloidal asymmetry of edge heating drives different turbulence spreading patterns and examine the underlying physical mechanisms that govern these nonlocal transport phenomena.

2. SIMULATION SETUP

In this study, we aim to analyze the nonlocal behavior of ITG turbulence and heat pulse using GYSELA. The initial setup follows the cyclone base case, and the system size of the simulation is $a/\rho_{ref}=180$, Corresponding Bohm-scale transport timescale is $t_{Bohm}\sim a^2/D_{Bohm}=(a/\rho_{ref})^2\omega_c^{-1}=3.24\times 10^4\omega_c^{-1}$. Here, ρ_{ref} is the reference Larmor radius for ion at r/a=0.5, and ω_c is reference gyrofrequency. Before implementing the poloidally localized heat source, we run the simulation for approximately $4t_{Bohm}$ after nonlinear saturation with a central heating source, to sufficiently relax the ion temperature profile. This is to maximize the effect of the poloidally localized heat source.

Fig. 1 shows the location of the poloidally localized heat source. We position it near the edge, where the region is relatively stable under the current simulation, and is suitable for analyzing nonlocal transport from the edge to the core. Note that heat source is toroidally symmetric. In addition, we maintain a region where turbulent fluctuations are artificially damped at 1.0 < r/a < 1.15 to enable the nonlocal propagation towards the outside. The amplitude of the source is set to the same magnitude as static source that maintains the existing profile, thereby maximizing the effects of this poloidally localized heat source. In this study, we mainly focus on in-out asymmetric behavior of turbulence and corresponding heat pulse propagation.

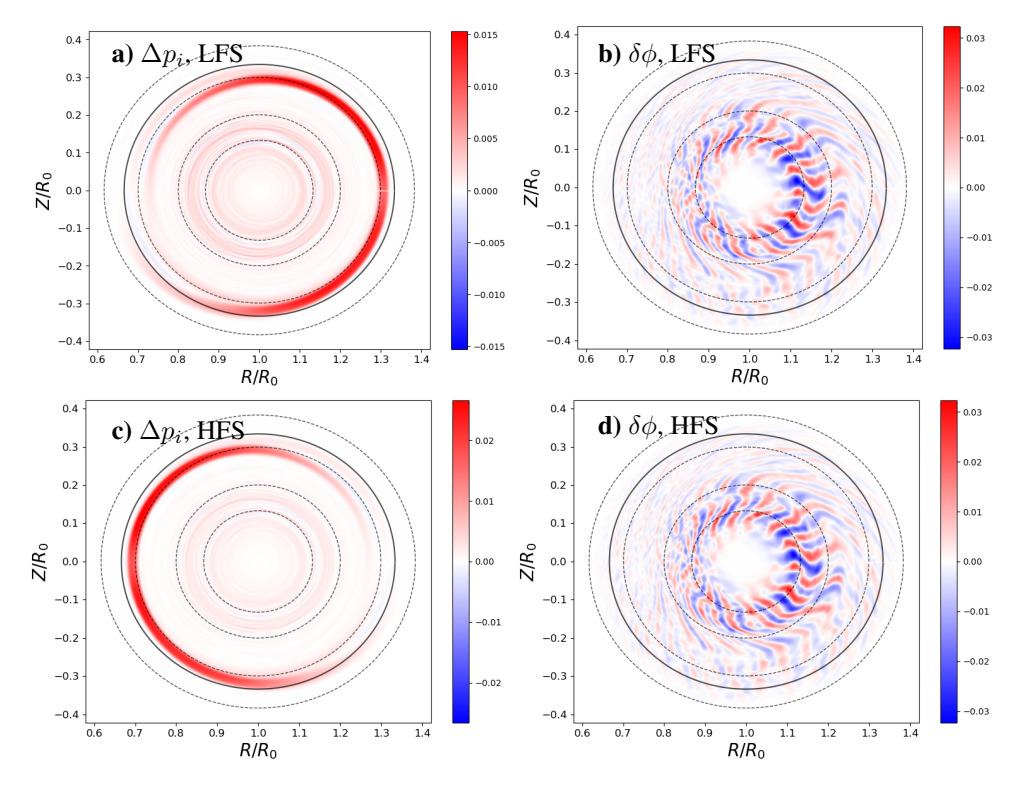


FIG. 2. Contour plots of (a, c) pressure increment Δp_i and (b, d) turbulent fluctuations $\delta \phi$ at $\Delta t = 1.5 \times 10^3 \omega_c^{-1}$ after the introduction of poloidally localized heat sources. Top panels (a, b): low field side heating. Bottom panels (c,d): high field side heating. Here, dashed lines represent r/a = 0.4, 0.6, 0.9, 1.15 and bold line represents r/a = 1.0.

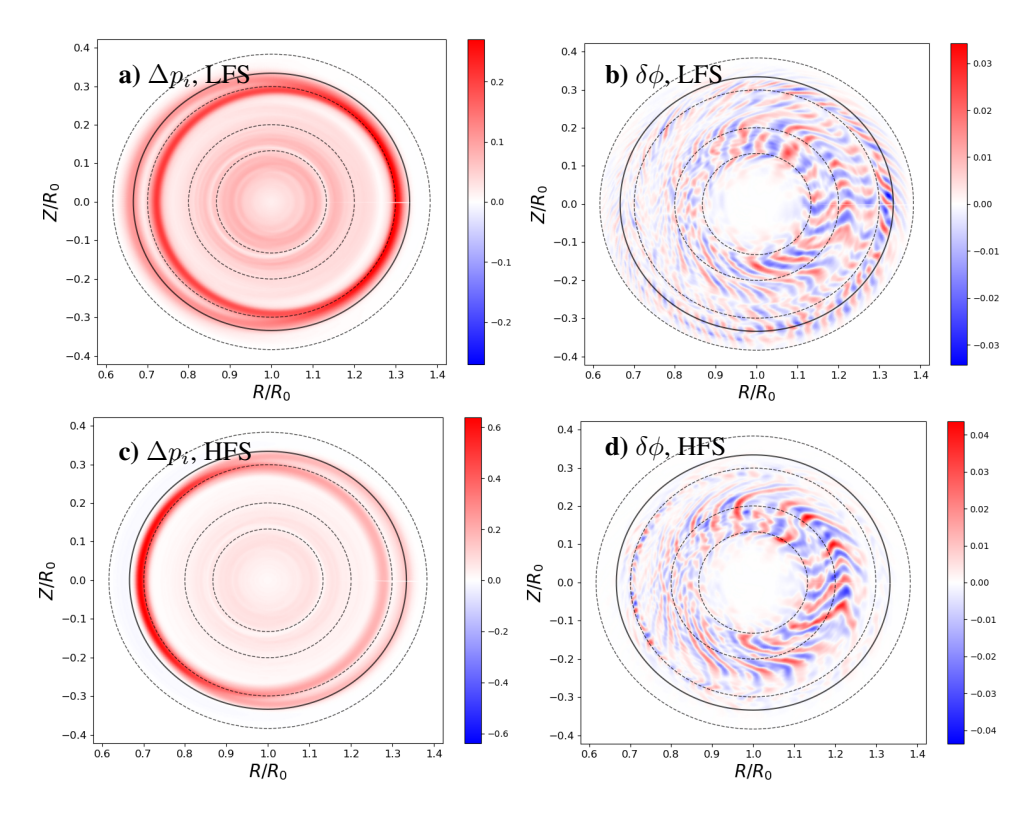


FIG. 3. Contour plots of (a, c) pressure increment Δp_i and (b, d) turbulent fluctuations $\delta \phi$ at $\Delta t = 7 \times 10^4 \omega_c^{-1}$ after the introduction of poloidally localized heat sources. Top panels (a, b): low field side (LFS) heating. Bottom panels (c,d): high field side (HFS) heating. Here, dashed lines represent r/a = 0.4, 0.6, 0.9, 1.15 and bold line represents r/a = 1.0.

3. IN-OUT ASYMMETRIC BEHAVIOR OF NONLOCAL TRANSPORT

First, we investigate the initial transport of both heat pulse and turbulent fluctuations when a poloidally localized heat source has been introduced. Figs. 2 a) and b) show the increment of pressure and turbulent fluctuation after $\Delta t = t_{measure} - t_{int} = 1.5 \times 10^3 \omega_c^{-1}$ when the heat source is applied on the low field side. Here, the turbulent fluctuation is $\delta \phi = \phi - \phi_{n=0}$, and the pressure increment is defined as $\Delta p_i = p_i(t_{measure}) - p_i(t_{int})$, where $t_{measure}$ is the time measured the quantities, and t_{int} is the time when the localized heat source is introduced. The heat pulse propagates from the low field side to the high field side. At this time, it shows a tendency to spread inward on the upside and outward on the downside. This occurs because, the parallel connection length at the edge is relatively long, making radial transfer due to magnetic curvature drift non-negligible. In current system size, $R_0 = 540 \rho_{ref}$, curvature drift velocity is roughly $v_{curv} \sim 2 \times 2 v_T^2/R\omega_c \sim 8 \times 10^{-3} v_T$. Multiplication of 2 comes from the target critical temperature of source. Therefore, the expected deviation is $\Delta t \times v_{curv} \sim 12 \rho_{ref}$, which shows agreement with the behavior of heat pulse. Meanwhile, turbulent fluctuations show little response initially, so that this radial shift is not due to the turbulent transport.

A similar trend is observed when the heat source is added on the high field side. Initially, Δp_i transfer shown in Fig. 2 c) from the high field side to the low field side occurs simultaneously on both the upside and downside. During this process, neoclassical transport causes the plasma to drift toward the core on the upside and toward the edge on the downside. Similar to the low field side heating case, turbulent fluctuations are not yet excited during this heat transfer process, so this transport can be explained by the combination of parallel transfer and magnetic curvature drift. It is noteworthy that this characteristic leads to the formation of a poloidally anisotropic pressure distribution.

Fig. 3 represents the results after $\Delta t = 7 \times 10^4 \omega_c^{-1}$, which is comparable to $2t_{Bohm}$. The pressure increment broadens and shows gaps on the high field side for low field side heating and on the low field side for high field side heating, which are due to magnetic curvature drift. This trend in pressure increment influences the turbulent fluctuations. Due to the poloidal anisotropy of the pressure profile, turbulent fluctuations become localized on the same side as the heating source: on the low field side for low field side heating and on the high field side for high field side heating. It is noteworthy that the anti-ballooning tendency is observed during high field side heating. Moreover, since the radial correlation length is longer on the low field side and generally exhibits ballooning

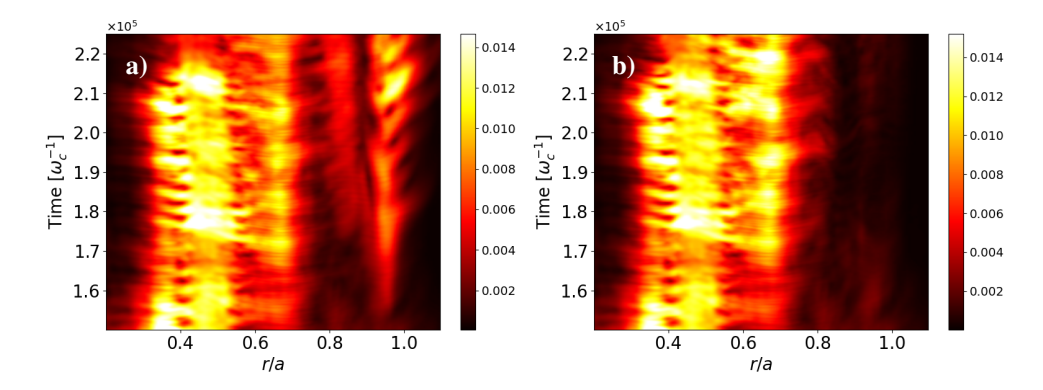


FIG. 4. 2D spectrum of $|\delta\phi|$ at low field side with $-30 < \theta < 30$ with respect to r/a and time. Here, heat source is introduced at a) the low field side and b) high field side.

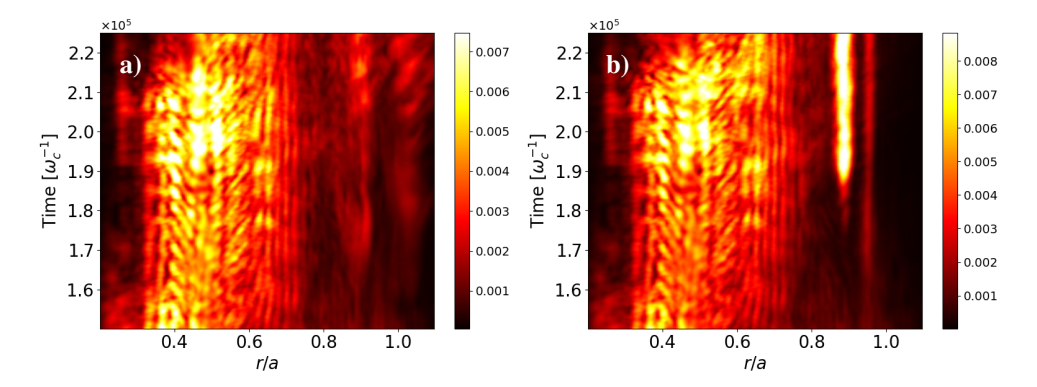


FIG. 5. 2D spectrum of $|\delta\phi|$ at high field side with $150 < \theta < 210$ with respect to r/a and time. Here, heat source is introduced at a) the low field side and b) high field side.

characteristics, low field side heating shows a tendency for turbulence spreading from the edge to the core in that region. However, such phenomena are difficult to confirm during high field side heating.

4. TURBULENCE SPREADING FORCED BY HEAT SOURCE

In this section, we estimate the turbulence spreading with respect to the location of edge heating. Fig. 4 shows the time evolution of turbulent fluctuations at the low field side, i.e. at poloidal angle θ where $-30 < \theta < 30$. For low field side heating, the excitation of $\delta \phi$ at $r/a \sim 0.9$ is observed, and it propagates towards both the core and edge direction. When turbulence spreads towards the core, the $E \times B$ shear layer, $\omega_{E \times B}$ in Fig. 6 a) also shifts radially towards the core. In contrast, no specific turbulence is observed in the high field side heating case. This becomes even more intriguing when compared with Fig. 5. In the low field side heating case, turbulence is observed at the $r/a \sim 0.9$ on the high field side as well, showing a similar pattern to that on the low field side. However, in the high field side heating case, extremely localized fluctuations are observed only on the high field side at the edge. This can be confirmed by comparing the pressure increment in Fig. 3 c). For high field side heating, relatively broader heating occurs on the low field side. Therefore, this region has lower linear gr compared to low field side heating. Moreover, since the $E \times B$ shearing rate tends to be stronger on the low field side even on the same flux surface[17], the $E \times B$ shearing effect is added to the linear damping, resulting in stronger local damping. Consequently, most of the turbulent fluctuations that would have been conducted in parallel are reduced due to this damping effect. Note that $\omega_{E \times B}$ in Fig. 6 b) shows strong barrier around $r/a \sim 0.9$. So, thermal and turbulent energy is locally confined at high field side.

5. CONCLUSION

In this study, we have investigated the nonlocal behavior of ITG turbulence and heat pulse propagation using GYSELA simulations with poloidally localized heat sources. Our analysis reveals asymmetries in turbulence spreading and heat transport depending on the heating location. The key findings are as follows: First, the initial heat pulse propagation is governed by parallel conduction and neoclassical drift effects, with magnetic curvature

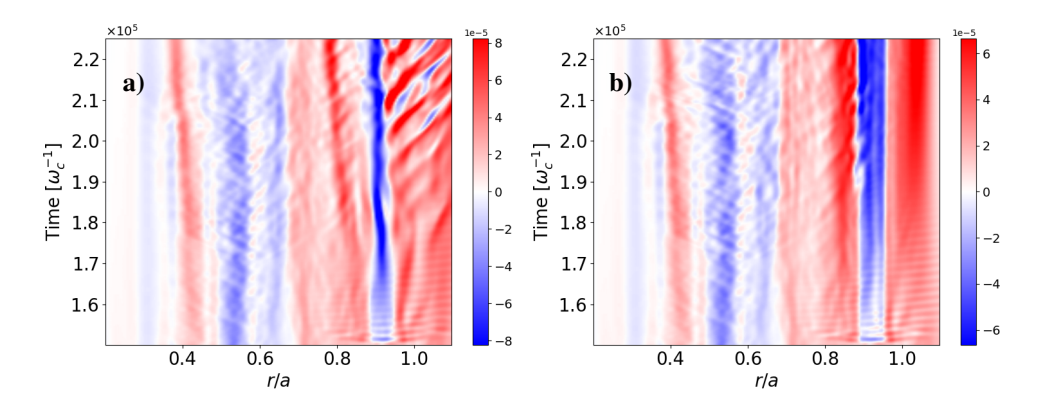


FIG. 6. 2D spectrum of $\omega_{E\times B}$ with respect to r/a and time. Here, heat source is introduced at a) the low field side and b) high field side.

drift playing a crucial role in creating poloidally inhomogeneous heat transfer. This anisotropy influences the subsequent turbulent response. Second, we observe a pronounced asymmetry in turbulence spreading between low field side and high field side heating scenarios. Low field side heating effectively excites turbulent fluctuations that propagate both toward the core and edge, accompanied by radial shifts in the $E \times B$ shear layer. This behavior is consistent with the ballooning characteristics of ITG turbulence, where longer radial correlation lengths on the low field side facilitate edge-to-core turbulence spreading.

In contrast, high field side heating produces highly localized fluctuations with minimal spreading capability. This suppression is attributed to the combined effects of broader pressure perturbations on the low field side and enhanced local damping due to stronger $E \times B$ shearing rates, which effectively reduce parallel conduction of turbulent fluctuations.

These results demonstrate that the poloidal location of edge heating critically determines the nonlocal transport characteristics, with implications for understanding heat pulse propagation and turbulence control strategies in tokamak plasmas.

ACKNOWLEDGEMENTS

This research is supported by the National Research Foundation, Singapore. The computational work is performed with computer and storage resources by National Supercomputing Centre(NSCC), Singapore (www.nscc.sg) and GENCI at TGCC thanks to the Grant 2024-A0160502224 on the super computer Joliot Curie's the SKL and ROME partition.

REFERENCES

¹X. Garbet, L. Laurent, A. Samain, and J. Chinardet, Nucl. Fusion **34**, 963 (1994).

²P. H. Diamond, V. B. Lebedev, D. E. Newman, and B. A. Carreras, Phys. Plasmas **2**, 3685 (1995).

³T. S. Hahm, P. H. Diamond, Z. Lin, K. Itoh, and S.-I. Itoh, Plasma Phys. Control. Fusion 46, A323 (2004).

⁴Ö. D. Gürcan, P. H. Diamond, T. S. Hahm, and Z. Lin, Phys. Plasmas **12**, 032303 (2005).

⁵X. Garbet, Y. Sarazin, F. Imbeaux, P. Ghendrih, C. Bourdelle, Ö. D. Gürcan, and P. H. Diamond, Phys. Plasmas **14**, 122305 (2007).

⁶T. S. Hahm and P. H. Diamond, J. Kor. Phys. Soc. **73**, 747 (2018).

⁷Z. Lin, S. Ethier, T. S. Hahm, and W. M. Tang, Phys. Rev. Lett. **88**, 195004 (2002).

⁸Z. Lin and T. S. Hahm, Phys. Plasmas **11**, 1099 (2004).

⁹B. F. McMillan, X. Lapillonne, S. Brunner, L. Villard, S. Jolliet, A. Bottino, T. Görler, and F. Jenko, Phys. Rev. Lett. **105**, 155001 (2010).

¹⁰S. Yi, J. M. Kwon, P. H. Diamond, and T. S. Hahm, Phys. Plasmas **21**, 092509 (2014).

¹¹S. Yi, J. M. Kwon, P. H. Diamond, and T. S. Hahm, Nucl. Fusion **55**, 092002 (2015).

¹²G. Dif-Pradalier, P. Ghendrih, Y. Sarazin, E. Caschera, F. Clairet, Y. Camenen, P. Donnel, X. Garbet, V. Grandgirard, Y. Munschy, L. Vermare, and F. Widmer, Commun. Phys. **5**, 229 (2022).

IAEA-CN-392/3096

- ¹³Y. Kosuga, P. H. Diamond, L. Wang, Ö. D. Gürcan, and T. S. Hahm, Nucl. Fusion **53**, 043008 (2013).
- ¹⁴M. Cao and P. H. Diamond, Phys. Rev. Lett. **134**, 235101 (2025).
- ¹⁵Z. Li, X. Chen, P. H. Diamond, X. Xu, X. Qin, H. Wang, F. Scotti, R. Hong, G. Yu, Z. Yan, F. Khabanov, and G. R. McKee, Commun. Phys. **7**, 96 (2024).
- ¹⁶Y. W. Cho, X. Garbet, R. Varennes, Z. S. Qu, P. Donnel, K. Obrejan, and V. Grandgirard, Nucl. Fusion 65, 036024 (2025).
- ¹⁷T. S. Hahm and K. H. Burrell, Phys. Plasmas **2**, 1648–1651 (1995).